

Metabolic Insights into Non-Alcoholic Fatty Liver Disease: Impact of Gut Microbiota and TCM Constitutions

Keywords

Gut Microbiota, Non-Alcoholic Fatty Liver Disease, Metabolic Pathways, Personalized Treatment, Traditional Chinese Medicine Constitution, 16S rRNA Sequencing

Abstract

Introduction

Metabolic dysfunction-associated steatotic liver disease (MASLD) is intricately linked to gut microbiota dysbiosis and is influenced by Traditional Chinese Medicine (TCM) constitution theory. This study explores the fecal microbiota composition in MASLD patients with varied TCM constitutions to unravel the molecular mechanisms underlying the disease.

Material and methods

In this study, 51 MASLD patients and 46 healthy controls were classified into seven TCM constitution groups based on high-throughput sequencing of fecal samples. Analyses were conducted to compare microbial communities, metabolite profiles, and metabolic pathways among these constitution groups. The relationships between specific microbiota and biochemical indicators were evaluated using LEfSe and Spearman correlation analyses.

Results

MASLD patients exhibited reduced fecal microbiota diversity compared to healthy controls, with significant variations in microbial structure among TCM constitution groups. The damp-heat constitution (DHC) and phlegm-dampness constitution (PDC) groups displayed enriched populations of specific microbial species, distinct bacterial taxa, and unique metabolite profiles. Multiple significant pathways related to amino acid, fatty acid, and carbohydrate metabolism were identified through metabolic pathway enrichment analysis. Significant correlations were observed between specific microbial taxa and biochemical indicators such as triglycerides, total cholesterol, alanine aminotransferase (ALT), and aspartate aminotransferase (AST).

Conclusions

This study highlights the close association between alterations in gut microbiota, TCM constitution differences, and MASLD progression. The findings suggest that changes in microbial diversity and metabolite profiles may play a crucial role in MASLD pathogenesis. The identification of constitution-specific microbial variations provides promising targets for personalized interventions and treatment strategies for MASLD.

1 **Metabolic Insights into Non-Alcoholic Fatty Liver Disease: Impact of**
2 **Gut Microbiota and TCM Constitutions**
3 **Running Title: TCM Constitution and Gut Microbiota in MASLD**
4
5

Preprint

6 Abstract

7 **Introduction:** Metabolic dysfunction-associated steatotic liver disease (MASLD) is intricately
8 linked to gut microbiota dysbiosis and is influenced by Traditional Chinese Medicine (TCM)
9 constitution theory. This study explores the fecal microbiota composition in MASLD patients with
10 varied TCM constitutions to unravel the molecular mechanisms underlying the disease.

11 **Materials and Methods:** In this study, 51 MASLD patients and 46 healthy controls were classified
12 into seven TCM constitution groups based on high-throughput sequencing of fecal samples.
13 Analyses were conducted to compare microbial communities, metabolite profiles, and metabolic
14 pathways among these constitution groups. The relationships between specific microbiota and
15 biochemical indicators were evaluated using LEfSe and Spearman correlation analyses.

16 **Results:** MASLD patients exhibited reduced fecal microbiota diversity compared to healthy
17 controls, with significant variations in microbial structure among TCM constitution groups. The
18 damp-heat constitution (DHC) and phlegm-dampness constitution (PDC) groups displayed enriched
19 populations of specific microbial species, distinct bacterial taxa, and unique metabolite profiles.
20 Multiple significant pathways related to amino acid, fatty acid, and carbohydrate metabolism were
21 identified through metabolic pathway enrichment analysis. Significant correlations were observed
22 between specific microbial taxa and biochemical indicators such as triglycerides, total cholesterol,
23 alanine aminotransferase (ALT), and aspartate aminotransferase (AST).

24 **Conclusions:** This study highlights the close association between alterations in gut microbiota,
25 TCM constitution differences, and MASLD progression. The findings suggest that changes in
26 microbial diversity and metabolite profiles may play a crucial role in MASLD pathogenesis. The
27 identification of constitution-specific microbial variations provides promising targets for
28 personalized interventions and treatment strategies for MASLD.

29 **Keywords:** Non-Alcoholic Fatty Liver Disease; Traditional Chinese Medicine Constitution; Gut
30 Microbiota; 16S rRNA Sequencing; Metabolic Pathways; Personalized Treatment

31 **Introduction**

32 Metabolic dysfunction-associated steatotic liver disease (MASLD) is the most prevalent
33 chronic metabolic stress-related liver disease worldwide, characterized by hepatic steatosis and lipid
34 accumulation [1], which can progress to liver cirrhosis and even hepatocellular carcinoma (HCC)
35 [2]. The global prevalence of MASLD is approximately 25% [3, 4], with a rising trend in China,
36 where the prevalence currently ranges from 15% to 30% [5], making it a significant public health
37 concern. The multifactorial etiology of MASLD involves genetic, metabolic, and environmental
38 factors, with the gut-liver axis playing a critical role in its pathogenesis. Enhancing the accuracy of
39 early diagnosis and timely intervention is essential to prevent disease progression and reduce the
40 secondary risk of HCC [6]. Furthermore, studies have shown that the gut microbiota and its
41 metabolites play pivotal roles in regulating metabolic processes, immune responses, and host
42 defenses, closely linking them to the development and progression of MASLD [7, 8]. Moreover,
43 increasing evidence indicates that environmental exposure to bisphenol compounds (such as BPA
44 and its derivatives) can induce hepatic fat accumulation, elevate the risk of MASLD/MAFLD, and
45 is closely associated with gut microbiota dysbiosis [9-11].

46 Recent studies have shown that the gut microbiota in MASLD patients exhibits significant
47 dysbiosis, such as an increased *Firmicutes/Bacteroidota* ratio and reduced levels of *Bacteroidota*
48 and *Ruminococcaceae* [8, 12]. Fecal microbiota transplantation experiments in high-fat diet-induced
49 MASLD mouse models further confirm the critical role of gut microbiota in the pathogenesis of
50 MASLD [13]. Additionally, gut microbial metabolites, including short-chain fatty acids (SCFAs,
51 such as acetate and butyrate), trimethylamine (TMA), bile acids (BA), and ethanol, directly
52 contribute to the mechanisms underlying MASLD [14, 15]. For example, SCFAs promote fatty acid
53 oxidation and inhibit hepatic lipid synthesis by activating adenosine monophosphate-activated
54 protein kinase (AMPK), thereby reducing hepatic fat accumulation [16]. These findings provide
55 new perspectives for MASLD prevention and treatment. However, current research primarily
56 focuses on microbial differences, lacking subgroup analyses based on individual patient

57 characteristics.

58 In Traditional Chinese Medicine (TCM) theory, the constitution is considered the foundation of
59 an individual's health, shaped by both innate endowment and acquired environment and is
60 characterized by relative stability and plasticity. Wang Qi's nine-type TCM constitution
61 classification system and diagnostic criteria hold significant importance in clinical prevention and
62 treatment. Studies have revealed that MASLD patients predominantly present with constitutions
63 such as yang deficiency constitution (YADC) and phlegm dampness, while liver qi stagnation
64 constitution (QSC), spleen deficiency, and internal damp-heat constitution (DHC) are also common
65 patterns [17]. The TCM concept that "the internal must have form, the external must have
66 manifestation" (from *Huangdi Neijing*) suggests that the constitution reflects internal physiological
67 changes and may have potential links with gut microbiota and metabolic characteristics [18, 19].
68 However, this relationship has yet to be thoroughly investigated in experimental research.

69 This study aims to explore the changes in the composition of the gut microbiota in MASLD
70 patients with different TCM constitution types and their association with metabolic characteristics.
71 By employing 16S rRNA high-throughput sequencing technology, the study seeks to reveal the
72 characteristic differences in the gut microbiota of MASLD patients with different constitution types.
73 Metabolomics data will be integrated to analyze variations in metabolite types and metabolic
74 pathways. Through this research, we aim to clarify the microbiota differences between different
75 constitution types and MASLD, providing a new theoretical foundation for the personalized
76 treatment of MASLD.

77

78 **Materials and Methods**

79 **Patient Cohort**

80 Between June 1, 2023, and March 1, 2024, this study enrolled 51 patients with MASLD and 49
81 age- and sex-matched healthy controls at our hospital. The study followed the ethical principles of

82 the Declaration of Helsinki and was approved by the Clinical Research Ethics Committee of
83 Changzhou Hospital of Traditional Chinese Medicine, affiliated with Nanjing University of Chinese
84 Medicine ([Approval Nos. 170043, B200357](#)). Inclusion and exclusion criteria are detailed in [Figure](#)
85 [S1](#). MASLD was diagnosed based on liver biopsy or imaging methods such as abdominal
86 ultrasound and computed tomography, following established diagnostic criteria. Healthy controls
87 had no history or symptoms of MASLD and had not used antibiotics, probiotics, or laxatives within
88 one month before participation. Individuals were excluded if they had fatty liver due to alcohol
89 intake (more than 140 g per week for males or 70 g for females), drug abuse, hereditary diseases,
90 other liver diseases including viral hepatitis or autoimmune liver disease, major chronic illnesses
91 such as malignancy, diabetes, or chronic kidney disease, were pregnant, or were unable to complete
92 stool sample collection or required assessments.

93 This study optimized constitution-based groups to ensure an adequate sample size and improve
94 statistical power. Due to small sample sizes in certain constitution groups (e.g., QSC, blood stasis
95 constitution (BSC), YADC, yin deficiency constitution (YIDC)), these were consolidated into two
96 groups: DHC and phlegm-dampness constitution (PDC). After adjustment, the effect size was set at
97 0.7, the significance level at 0.05, and the statistical power at 0.8. Based on these statistical
98 calculations, the sample size of 51 MASLD patients was sufficient to meet the needs of this
99 exploratory study, ensuring the statistical validity of the analyses.

100

101 **Clinical Characteristics and Data Collection**

102 The clinical characteristics of MASLD patients and healthy controls were assessed using
103 standardized procedures at Changzhou Traditional Chinese Medicine Hospital, affiliated with
104 Nanjing University of Chinese Medicine. Sample collection was conducted by trained laboratory
105 technicians who adhered strictly to standardized protocols. Fasting venous blood samples were
106 collected from participants in the morning. After collection, laboratory staff immediately
107 centrifuged blood samples to separate the serum, which was then stored at -80°C until further

108 analysis. Lipid parameters, TG, TC, high-density lipoprotein cholesterol (HDL-C), and low-density
109 lipoprotein cholesterol (LDL-C), were measured using enzymatic methods on a fully automated
110 biochemical analyzer (Beckman Coulter AU5800, USA). Liver function indicators, such as ALT,
111 AST, alkaline phosphatase (ALP), and gamma-glutamyl transferase (GGT), were also analyzed
112 using the same equipment and standardized methods. Clinical nurses recorded patient demographic
113 information, including gender, age, height, and weight, at enrollment, and body mass index (BMI)
114 was calculated. All data collection and testing adhered strictly to the hospital's quality control
115 procedures, ensuring the accuracy and consistency of the results.

116

117 **Assessment of TCM Constitution**

118 During patient enrollment, this study applied *the Classification and Determination of*
119 *Constitution of Traditional Chinese Medicine* developed by *the Chinese Association of Traditional*
120 *Chinese Medicine* to assess the TCM constitution of all participants, ensuring scientific rigor and
121 classification accuracy. The specific procedure includes the following steps: First, two TCM experts
122 conduct consultations and observations of the patients, collecting information on tongue coating,
123 complexion, body shape, and pulse condition. Next, participants complete a standardized
124 *Traditional Chinese Medicine Constitution Classification Questionnaire*, where the nine basic
125 constitution characteristics (balanced constitution, qi deficiency constitution (QDC), YADC, YIDC,
126 PDC, DHC, BSC, QSC, and inherited special constitution) are quantified using a Likert 5-point
127 scale. Then, based on the questionnaire scores and clinical manifestations, a unified determination
128 formula is used to classify patients into a specific constitution. For example, if a constitution type
129 scores above 40 points and others score below 30, the patient is classified into that constitution. If
130 multiple constitution types score above 30 points, an expert panel integrates clinical manifestations
131 to comprehensively determine the constitution type. To ensure classification consistency, a subset of
132 patients (n=20) was reassessed within one week, and the results showed a Kappa value of 0.82,
133 indicating high reliability of the classification.

134

135 **Sample Collection**

136 Fecal samples were collected for gut microbiota analysis and metabolomics research. The
137 sample collection took place in a designated collection room at Changzhou Traditional Chinese
138 Medicine Hospital, affiliated with Nanjing University of Chinese Medicine. Each participant
139 received detailed instructions on the collection process, and trained professionals assisted with the
140 procedure. Participants collected fresh fecal samples in a designated area using single-use sterile
141 sampling tubes to prevent external contamination. After collection, healthcare staff immediately
142 placed the samples in liquid nitrogen to prevent degradation or metabolic changes in the microbiota.
143 All samples were stored at -80°C until they were transported to Shenzhen Microbiota Technology
144 Co. for high-throughput sequencing analysis.

145

146 **DNA Extraction and 16S rRNA Sequencing**

147 Total DNA from fecal samples was extracted using the EZNA® Soil Kit (Omega Bio-tek,
148 Norcross, USA). DNA purity and concentration were measured using the NanoDrop 2000, and
149 extraction quality was assessed by 1% agarose gel electrophoresis. The extraction process was
150 strictly controlled in a sterile environment, with all experimental steps carried out in a laminar flow
151 hood and using sterilized consumables to ensure the integrity and contamination-free status of the
152 DNA samples. Polymerase chain reaction (PCR) amplification targeted the V3-V4 hypervariable
153 regions, using primers 338F (5'-ACTCCTACGGGAGGCAGCAG-3') and 806R
154 (5'-GGACTACHVGGGTWTCTAAT-3'). The 20 µL PCR reaction mixture consisted of 9 µL sterile
155 double-distilled water, 4 µL 5FastPfu buffer, 2 µL 2.5 mM dNTPs, 0.8 µL of each 5 mM primer, 0.4
156 µL FastPfu polymerase, and 10 ng of DNA template. The thermal cycling program included an
157 initial denaturation at 95°C for 3 minutes, followed by 27 cycles of 95°C for 30 seconds, 55°C for
158 30 seconds, and 72°C for 45 seconds, with a final extension at 72°C for 10 minutes (PCR
159 instrument: ABI GeneAmp® 9700). PCR products were separated by 2% agarose gel

160 electrophoresis and purified using the AxyPrep DNA Gel Extraction Kit (Axygen Biosciences,
161 Union City, USA). Elution was performed with Tris-HCl, and the purified products were verified by
162 2% agarose gel electrophoresis. DNA quantification was performed using the QuantiFluor™-ST
163 system (Promega, USA). The purified amplicons were subjected to dual-end (PE) 2300 library
164 construction following the standard protocol for the Illumina MiSeq platform (Illumina, San Diego,
165 USA). During sequencing, each sample was ensured to have at least 50,000 valid sequence reads to
166 meet the depth requirements for microbiota diversity analysis.

167

168 **Microbiota Analysis via 16S rDNA Sequencing**

169 Sequence read processing, quality control, OTU clustering, and taxonomic assignment were
170 performed using the QIIME pipeline (v1.9.0). Adapter sequences and low-quality reads were
171 removed with Trimmomatic (v0.39), ensuring Q30 quality (error rate <0.1%) and discarding reads
172 shorter than 100 bp. Low-quality bases at the 3' end were trimmed using PRINSEQ (v0.20.4), and
173 paired-end reads were merged with fastq-join. Sequence quality was assessed using FastQC
174 (v0.11.9), and chimeric sequences were removed with USEARCH 6.1.544. OTUs were clustered
175 using UCLUST at 97% similarity and aligned to the Greengenes reference database (v13.8).
176 Taxonomic classification at the genus level was based on 97% sequence similarity using the
177 Greengenes (gg_13_8) database. Alpha diversity metrics, including the Shannon index, observed
178 species, and Chao1 index, were calculated in QIIME. Principal Coordinates Analysis (PCoA) using
179 weighted and unweighted UniFrac distances and PERMANOVA were also conducted in QIIME.
180 Differential taxa analysis was performed with LEfSe (Galaxy v1.0, The Huttenhower Lab, Harvard
181 T.H. Chan School of Public Health), using an LDA score threshold of 2.0 and a significance level of
182 $p < 0.05$ to ensure statistical robustness and biological relevance.

183

184 **Statistical Analysis of Clinical Data**

185 Baseline characteristics were analyzed using descriptive statistics. Quantitative variables are

186 presented as standard deviation (SD) or interquartile range (IQR), while categorical variables are
187 expressed as percentages. Differences in clinical indicators between groups were assessed using the
188 χ^2 test. Depending on the distribution, the Student's t-test or the Wilcoxon rank-sum test was applied
189 for continuous variables. Univariate logistic regression was used to estimate crude odds ratios and
190 their corresponding 95% confidence intervals.

191

192 **GC TOF-MS Experiment**

193 GC-TOF-MS analysis was conducted using an Agilent 7000D GC/MS system (Trace
194 1310-TSQ8000 Evo, Thermo Fisher Scientific, USA) equipped with a TG-5MS capillary column
195 coated with 5% diphenyl and 95% dimethylpolysiloxane. A 1 μ L sample was injected in split mode,
196 with helium as the carrier gas. The front inlet purge flow rate was set at 3 mL/min, and the column
197 flow rate at 1 mL/min. The oven temperature was initially held at 60°C for 1 minute, then increased
198 at 10°C/min to 320°C, where it was maintained for 14 minutes. The injector, transfer line, and ion
199 source temperatures were maintained at 280°C, 280°C, and 250°C, respectively. Electron impact
200 ionization was used with an ionization energy of -70 eV. Data were acquired in full scan mode (m/z
201 50-500) at a scan rate of 20 spectra per second, with a solvent delay beginning at 6.27 minutes.
202 Each sample was analyzed in triplicate, and internal standards were added to normalize peak
203 intensities and ensure reproducibility.

204

205 **GC-MS Data Preprocessing**

206 MS-DIAL software performed peak extraction, baseline filtering, baseline calibration, peak
207 alignment, deconvolution, and peak identification. Following this, peak area integration and mass
208 spectrometry matching were carried out. Metabolite identification was performed by comparing
209 with the NIST 17 and Fiehn databases to ensure the accuracy of the identification results. A data
210 matrix was then generated, and the raw spectral files underwent preprocessing. The criteria for
211 differential metabolite selection were fold change (FC) >1.2 or <0.8333 , with a *p*-value set to <0.05 .

212 To enhance the statistical significance of metabolite identification, multiple testing correction was
213 applied to the selected results using the Benjamini-Hochberg method.

214

215 **Microbiota Statistical Analysis**

216 The Shannon index, observed species, and Chao1 index, which are α -diversity metrics, were
217 assessed using Student's t-test. β -diversity was measured using UniFrac distance, and statistical
218 analysis was conducted using the chi-square test or PERMANOVA. Statistical significance was
219 defined as a p -value ≤ 0.05 .

220

221 **Metabolomics Data Analysis**

222 The Wilcoxon rank-sum test and FC analysis assessed differences in fecal metabolites between
223 the DHC and PDC groups. Differential metabolites were then aligned with metabolic pathways by
224 comparing them to the Kyoto Encyclopedia of Genes and Genomes (KEGG) database. A pathway
225 was considered enriched if more than three metabolites were mapped to it, and the enrichment
226 factor was calculated accordingly.

227

228 **Results**

229 **Baseline Characteristics of Study Participants and TCM Constitution Classification**

230 This study included 51 MASLD patients and 46 healthy controls. MASLD patients were
231 classified according to TCM constitution into the following groups: DHC (n=14), PDC (n=28),
232 QDC (n=3), QSC (n=1), BSC (n=2), YADC (n=1), and YIDC (n=2). Healthy controls did not show
233 significant skewed constitution traits. Gender, age, and key clinical characteristics of both groups
234 are summarized in [Table 1](#). MASLD patients had significantly higher BMI than healthy controls.
235 However, no significant BMI differences were observed among the constitution subgroups ($p >$
236 0.05). Triglyceride (TG) levels were elevated in the MASLD group compared to controls ($p < 0.05$),

237 particularly in the DHC group (2.56 ± 1.41 mmol/L) and PDC group (3.8 ± 1.67 mmol/L). HDL-C
238 levels also differed significantly across constitution groups ($p < 0.05$), with the PDC group showing
239 the lowest levels (0.56 ± 0.04 mmol/L) and the DHC group slightly higher (1.01 ± 0.27 mmol/L).

240 Liver function indicators, including AST and ALT, were elevated in MASLD patients. The
241 highest ALT was observed in the PDC group (57.42 ± 60.06 U/L), while the DHC group had lower
242 levels (28.73 ± 21.09 U/L; $p > 0.05$). Glucose (GLU) levels were increased in the PDC group (9.78
243 ± 2.07 mmol/L), though the difference among constitution groups was not statistically significant
244 ($p > 0.05$). The clinical data indicate distinct metabolic patterns among MASLD patients with
245 different TCM constitutions, with DHC and PDC groups showing more pronounced changes.

246

247 **Diversity Changes in the Fecal Microbiota of MASLD Patients**

248 To assess gut microbiota diversity and richness across different TCM constitution groups,
249 α -diversity analysis was conducted using the Shannon, Ace, Chao1, and Simpson indices (Figure
250 1A-D). The results showed variability in diversity metrics among constitution groups. The DHC and
251 PDC groups exhibited higher Chao1 and Shannon indices, indicating greater microbial diversity and
252 richness, while the QDC group had relatively lower values. Boxplot distributions of the Ace and
253 Chao1 indices suggested increased species richness in the YIDC group, potentially reflecting
254 constitution-specific microbial traits. However, none of the differences reached statistical
255 significance ($p > 0.05$), suggesting overall microbial diversity remained relatively stable across
256 groups.

257 Principal Component Analysis (PCA) and Non-metric Multidimensional Scaling (NMDS)
258 based on Bray-Curtis distances were performed to explore differences in microbiota composition.
259 PCA revealed distinct clustering patterns in the DHC and PDC groups, separating them clearly from
260 other constitution types. In contrast, groups such as QDC and QSC showed more dispersed
261 distributions, indicating greater internal heterogeneity in microbiota structure (Figure 2A). NMDS
262 analysis supported the PCA findings, further confirming the compositional similarity and clustering

263 observed in the DHC and PDC groups (Figure 2B).

264

265 **Taxonomic Differences in Microbiota Among Different TCM Constitution Groups**

266 Venn diagram analysis was used to assess the distribution of ASVs (Amplicon Sequence
267 Variants) across different constitution groups (Figure 3A). The PDC group showed the highest
268 number of ASVs (8620), followed by DHC (3386), YIDC (843), QDC (736), BSC (529), YADC
269 (208), and QSC (168). A total of 23 core ASVs were shared across all groups.

270 The relative abundance of microbial taxa was visualized using stacked bar charts. At the
271 phylum level (Figure 3B), *Bacteroidota*, *Proteobacteria*, and *Firmicutes* were dominant in all
272 groups. *Bacteroidota* was reduced in the YIDC group, while *Proteobacteria* were notably higher in
273 the QDC and YIDC groups. *Firmicutes* abundance was relatively increased in YIDC. At the class
274 level (Figure 3C), *Bacteroidetes*, *Clostridium*, *Negativicutes*, *Gamma Proteobacteria*, and *Bacilli*
275 were the major taxa. The YIDC group showed lower *Bacteroidota* and higher levels of *Firmicutes*
276 and *Gamma Proteobacteria*. At the order level (Figure 3E), *Lachnospirales* abundance was elevated
277 in the QDC and YIDC groups. *Oscillospira* was lowest in the YADC group. *Enterobacteriales* was
278 increased in the QDC, QSC, and YIDC groups. At the genus level (Figure 3D), *Bacteroides* was
279 predominant in all groups, with higher levels in PDC and DHC. *Blautia* and *Dialister* were enriched
280 in the QDC group. The YIDC group had the lowest *Faecalibacterium* and higher proportions of
281 *Gamma Proteobacteria* and *Enterobacteriales*. *Lachnoclostridium* was more abundant in PDC and
282 DHC, while *Prevotella* was enriched in DHC. *Oscillospira* showed the lowest abundance in the
283 YADC group. These findings indicate distinct genus-level profiles across constitution groups.

284

285 **Correlation Between Gut Microbiota and Clinical Biochemical Indicators**

286 LEfSe analysis (with an LDA threshold set at 2) identified bacterial taxa significantly different
287 across various constitution groups (Figure 4A-B). The results revealed that *Parabacteroides*
288 characterized the BSC group as the dominant genus, while the YADC group showed the highest

289 abundance of *Clostridium*. The YIDC group had unique bacterial features, with *Cellulosilyticum*,
290 *Dorea*, and *Prevotella* being the most significant characteristic genera, with LDA scores greater
291 than 3.

292 Further Spearman correlation analysis was performed to evaluate the relationships between gut
293 microbiota and clinical biochemical indicators (Figure 4C). At the phylum level, TG, TC, ALT, AST,
294 and GLU were significantly positively correlated with *Ayanobacteriota* ($p < 0.05$). Additionally, at
295 the order level, TG and TC were positively correlated with *Cyanobacteria* ($p < 0.05$), while GLU,
296 ALT, and AST were positively correlated with *Acidobacteria* and *Thermoleophilia* ($p < 0.05$). GLU
297 was negatively correlated with *Bacilli* ($p < 0.05$). At the genus level, AST positively correlated with
298 UCG-002 ($p < 0.05$).

299

300 **Fecal Metabolomic Features of MASLD Patients**

301 Figure 5 presents the total ion chromatograms of fecal samples from the PDC and DHC groups,
302 with the strongest chromatographic peaks set at 100% relative abundance, reflecting the overall
303 distribution characteristics of the fecal metabolites in both groups. The chromatograms show sharp
304 peaks and good separation, with most metabolites detected between 5 and 19 minutes. Significant
305 differences in peak intensities were observed between the groups: the PDC group exhibited higher
306 peak intensities at 10.44 minutes and 17.35 minutes, while the DHC group showed higher peak
307 intensities at 6.17 minutes and 18.51 minutes. Metabolite identification was conducted using
308 MS-DIAL and the NIST database, leading to the identification of 106 metabolites, including small
309 molecules such as amino acids and fatty acids.

310

311 **Metabolite Differential Analysis Among Different TCM Constitution Groups**

312 The PCA score plot (Figure 6A) shows significant spatial separation between the metabolite
313 profiles of the DHC and PDC groups, indicating strong metabolic differences between the two
314 groups. Further analysis using a volcano plot (Figure 6B, Table 2) with the thresholds of $p < 0.05$

315 and $FC > 1.5$ or < 0.667 revealed a total of 106 differential metabolites. Among the top 20
316 metabolites identified were lyxose, arabitol, iminodiacetic acid, quercetin, quinic acid, putrescine,
317 sucrose, 1,2,4-benzenetriol, succinic acid, 4-hydroxy-3-methoxybenzoic acid, 4-nitro catechol,
318 glycerol-1-phosphate, inosine, O-phospho-serine, uracil, 4-pyridoxine, hydroquinone, caffeic acid,
319 gallic acid, and 4-hydroxybenzoic acid. Notably, lyxose, arabitol, and iminodiacetic acid exhibited
320 significant statistical differences ($p < 0.05$), suggesting their important role in distinguishing the
321 DHC and PDC groups. Heatmap analysis ([Figure 6C](#)) further revealed clear clustering patterns in
322 the metabolite expression profiles between the DHC and PDC group samples, showing distinct
323 metabolic patterns between the two groups.

324

325 **Functional Annotation of Differential Metabolites and Enrichment of Metabolic Pathways**

326 Metabolic pathway enrichment analysis of differential metabolites between the DHC and PDC
327 groups identified 15 significantly associated pathways ([Figure 7, Table 3](#)). Among them, the
328 biosynthesis of phenylalanine, tyrosine, and tryptophan (Pathway 1) and the metabolism of glycine,
329 serine, and threonine (Pathway 2) showed the highest enrichment and topological impact, located in
330 the upper right quadrant of the pathway topology plot. Pathway 1 and Pathway 2 were both
331 significantly enriched and exhibited high centrality within the metabolic network, indicating their
332 potential involvement in the major metabolic distinctions between the DHC and PDC groups. Other
333 pathways, including ascorbate metabolism and alanine, aspartate, and glutamate metabolism, also
334 showed moderate enrichment, though with lower topological impact values. These results suggest
335 that amino acid and energy metabolism pathways are key contributors to the metabolic differences
336 between the two constitution types.

337

338 **Discussion**

339 MASLD is a common metabolic liver disease ($\geq 5\%$ hepatic fat) unrelated to alcohol [[14, 20](#)],

340 affecting 25%-45% of the global population and increasingly younger individuals [21, 22]. This
341 study, integrating microbiomics and metabolomics, reveals TCM constitution-specific gut and
342 metabolic signatures in MASLD (DHC, PDC), highlighting microbiota diversity loss and pathway
343 shifts as key mechanisms, and offering novel insights for personalized intervention.

344 Results showed that MASLD patients exhibited reduced gut microbiota diversity and
345 significant alterations in microbial composition, including increased relative abundances of
346 *Firmicutes* and *Proteobacteria*, decreased *Bacteroidetes*, and a disrupted *Firmicutes/Bacteroidota*
347 ratio [23]. At the constitution subtype level, microbiota profiles differed between DHC and PDC
348 types. Notably, both groups showed elevated *Proteobacteria*, potentially linked to increased
349 intestinal permeability and inflammation. From a TCM perspective, this may reflect a microbial
350 distinction between "excess" and "deficiency" syndromes. Metabolomic analysis further revealed
351 significant differences in glycine and aspartic acid levels between constitutions, suggesting a role in
352 oxidative stress and energy metabolism regulation [24].

353 Further studies also confirmed constitution-specific gut microbiota signatures in NAFLD. The
354 PDC group exhibited more pronounced dysbiosis, characterized by a lower
355 *Firmicutes/Bacteroidetes* ratio, reduced *Faecalibacterium*, and elevated *Prevotella* features
356 associated with inflammation and metabolic disruption [25]. Additionally, *Flavonifractor plautii*
357 and its metabolite phytosphingosine were significantly reduced in PDC individuals, leading to
358 decreased PPAR α pathway activity in the liver and aggravating lipid metabolic disorders, even in
359 individuals without overt metabolic abnormalities, indicating a high-risk metabolic profile [26]. In
360 contrast, DHC patients showed elevated serum bile acids and downregulated protein expression,
361 suggesting impaired systemic immune regulation and gut-liver axis dysfunction [27].

362 Both PDC and DHC types showed enrichment in amino acid metabolic pathways, particularly
363 those involving phenylalanine, tyrosine, glycine, and serine pathways implicated in oxidative stress,
364 energy homeostasis, and inflammation [28]. The PDC group also showed increased metabolites
365 such as lyxose and arabitol, reflecting enhanced carbohydrate metabolism [29]. Proteomic data

366 further indicated that PDC patients tended to activate JAK–STAT and PI3K-Akt signaling, whereas
367 DHC patients showed downregulation of immune-related proteins, suggesting constitution-specific
368 differences in inflammatory and metabolic susceptibility [30]. Collectively, this study elucidates a
369 constitution-microbiota-metabolism axis in MASLD, demonstrating distinct microbial, metabolic,
370 and signaling features in DHC and PDC subtypes. These findings support personalized
371 microbiota-targeted strategies based on constitution, such as modulating specific microbes or
372 supplementing key metabolites, to enable precise prevention and treatment of MASLD.

373 Despite these novel findings, several limitations exist. First, sample sizes for less common
374 constitutions (e.g., Qi stagnation, blood stasis, yang deficiency, yin deficiency) were small, and
375 group merging may have obscured subtle differences. Second, 16S rRNA sequencing has limited
376 taxonomic resolution and relies on predictive functional annotation, lacking direct functional
377 evidence [31]. Third, participants were recruited from a single geographic region, and their gut
378 microbiota may be influenced by local diet, lifestyle, and environment, which limits generalizability.
379 Previous studies suggest gut microbial changes may precede MASLD progression, emphasizing the
380 need for time-series and multi-omics approaches [32], alongside standardized dietary assessments to
381 reduce bias [33].

382 TCM constitution classification also remains partly subjective, despite existing criteria.
383 Integrating genomics, epigenetics, and immunophenotyping could help identify objective
384 biomarkers and enhance scientific rigor and global recognition of TCM constitution research [34].
385 Furthermore, liver function markers like serum albumin should be included, as albumin not only
386 reflects hepatic synthesis capacity but also exhibits esterase-like activity involved in lipid
387 metabolism [35]; its reduction in NAFLD is associated with disease progression and dysbiosis [36].
388 Future research should incorporate metagenomics, transcriptomics, metabolomics, and single-cell
389 technologies, along with germ-free animals, liver organoids, and in vitro models, to functionally
390 validate constitution-related microbes and metabolites. Developing MASLD subtyping models
391 based on TCM constitutions and confirming causality through animal and clinical studies will help

392 bridge TCM theory with precision medicine and promote individualized interventions in MASLD.

393

394 **Conclusion**

395 This study revealed significant differences in the gut microbiota composition and metabolic
396 characteristics of MASLD patients with different TCM constitutions, particularly in DHC and PDC,
397 showing constitution-specific changes in the microbiota ([Graphic abstract](#)). The associations
398 between clinical indicators such as blood lipids and liver function with specific microbiota suggest
399 that gut microbiota diversity and stability may be key factors in the pathology of MASLD. These
400 findings provide potential microbial targets for constitution-related personalized diagnosis and
401 treatment of MASLD.

402

403 **Abbreviations**

404 AMPK: Adenosine Monophosphate-Activated Protein Kinase

405 ALP: Alkaline Phosphatase

406 ALT: Alanine Aminotransferase

407 AST: Aspartate Aminotransferase

408 BA: Bile Acids

409 BMI: Body Mass Index

410 BSC: Blood Stasis Constitution

411 DHC: Damp-Heat Constitution

412 FC: Fold Change

413 GGT: Gamma-Glutamyl Transferase

414 GLU: Glucose

415 HCC: Hepatocellular Carcinoma

416 HDL-C: High-Density Lipoprotein Cholesterol

417 IQR: Interquartile Range

418 KEGG: Kyoto Encyclopedia of Genes and Genomes

419 LDA: Linear Discriminant Analysis

420 LDL-C: Low-Density Lipoprotein Cholesterol

421 MASLD: Metabolic Dysfunction-Associated Steatotic Liver Disease

422 NMDS: Non-Metric Multidimensional Scaling

423 PCA: Principal Component Analysis

424 PCoA: Principal Coordinates Analysis

425 PCR: Polymerase Chain Reaction

426 PDC: Phlegm-Dampness Constitution

427 PE: Dual-End

428 QDC: Qi Deficiency Constitution

429 QSC: Qi Stagnation Constitution

430 SCFAs: Short-Chain Fatty Acids

431 SD: Standard Deviation

432 TC: Total Cholesterol

433 TCA: Tricarboxylic Acid

434 TCM: Traditional Chinese Medicine

435 TG: Triglycerides

436 TMA: Trimethylamine

437 YADC: Yang Deficiency Constitution

438 YID: Yin Deficiency Constitution

439 **References**

440 1. Gerges SH, Wahdan SA, Elsherbiny DA, El-Demerdash E. Non-alcoholic fatty liver disease:
441 An overview of risk factors, pathophysiological mechanisms, diagnostic procedures, and
442 therapeutic interventions. *Life Sciences*. 2021;271:119220. doi:10.1016/j.lfs.2021.119220

443 2. Dou L, Shi X, He X, Gao Y. Macrophage Phenotype and Function in Liver Disorder. *Front*
444 *Immunol*. 2020;10. doi:10.3389/fimmu.2019.03112

445 3. Draijer L, Benninga M, Koot B. Pediatric NAFLD: an overview and recent developments in
446 diagnostics and treatment. *Expert Review of Gastroenterology & Hepatology*.
447 2019;13(5):447-461. doi:10.1080/17474124.2019.1595589

448 4. Powell EE, Wong VWS, Rinella M. Non-alcoholic fatty liver disease. *The Lancet*.
449 2021;397(10290):2212-2224. doi:10.1016/s0140-6736(20)32511-3

450 5. Govaere O, Petersen SK, Martinez-Lopez N, et al. Macrophage scavenger receptor 1 mediates
451 lipid-induced inflammation in non-alcoholic fatty liver disease. *Journal of Hepatology*.
452 2022;76(5):1001-1012. doi:10.1016/j.jhep.2021.12.012

453 6. Jiang W, Wu N, Wang X, et al. Dysbiosis gut microbiota associated with inflammation and
454 impaired mucosal immune function in intestine of humans with non-alcoholic fatty liver disease. *Sci*
455 *Rep*. 2015;5(1). doi:10.1038/srep08096

456 7. Aron-Wisnewsky J, Vigliotti C, Witjes J, et al. Gut microbiota and human NAFLD:
457 disentangling microbial signatures from metabolic disorders. *Nat Rev Gastroenterol Hepatol*.
458 2020;17(5):279-297. doi:10.1038/s41575-020-0269-9

459 8. Oh TG, Kim SM, Caussy C, et al. A Universal Gut-Microbiome-Derived Signature Predicts
460 Cirrhosis. *Cell Metabolism*. 2020;32(5):878-888.e6. doi:10.1016/j.cmet.2020.06.005

461 9. Gill K, Bindal E, Garg P, Kumar D, Bhattacharyya R, Banerjee D. Exposure of Bisphenols
462 (BPA, BPB and BPC) in HepG2 Cells Results in Lysosomal Dysfunction and Lipid Accumulation.
463 *Cell Biology International*. 2025;49(6):709-722. doi:10.1002/cbin.70017

464 10. Li CL, Yao ZY, Zhang YF, et al. Bisphenols exposure and non-alcoholic fatty liver disease:

465 from environmental trigger to molecular pathogenesis. *Front Endocrinol.* 2025;16.
466 doi:10.3389/fendo.2025.1606654

467 11. Feng D, Zhang H, Jiang X, et al. Bisphenol A exposure induces gut microbiota dysbiosis and
468 consequent activation of gut-liver axis leading to hepatic steatosis in CD-1 mice. *Environmental*
469 *Pollution*. 2020;265:114880. doi:10.1016/j.envpol.2020.114880

470 12. JASIRWAN COM, MURADI A, HASAN I, SIMADIBRATA M, RINALDI I. Correlation
471 of gut Firmicutes/Bacteroidetes ratio with fibrosis and steatosis stratified by body mass
472 index in patients with non-alcoholic fatty liver disease. *Bioscience of Microbiota, Food*
473 *and Health*. 2021;40(1):50-58. doi:10.12938/bmfh.2020-046

474 13. Yu JS, Youn GS, Choi J, et al. Lactobacillus lactis and Pediococcus pentosaceus-driven
475 reprogramming of gut microbiome and metabolome ameliorates the progression of non-alcoholic
476 fatty liver disease. *Clinical & Translational Med.* 2021;11(12). doi:10.1002/ctm2.634

477 14. Zhu M, Dagah OMA, Silaa BB, Lu J. Thioredoxin/Glutaredoxin Systems and Gut
478 Microbiota in NAFLD: Interplay, Mechanism, and Therapeutical Potential. *Antioxidants*.
479 2023;12(9):1680. doi:10.3390/antiox12091680

480 15. Nowiński A, Ufnal M. Gut bacteria-derived molecules as mediators and markers in
481 cardiovascular diseases. The role of the gut-blood barrier. *Kardiol Pol.* 2018;76(2):320-327.
482 doi:10.5603/kp.a2017.0204

483 16. Loomba R, Seguritan V, Li W, et al. Gut Microbiome-Based Metagenomic Signature for
484 Non-invasive Detection of Advanced Fibrosis in Human Nonalcoholic Fatty Liver Disease. *Cell*
485 *Metabolism*. 2019;30(3):607. doi:10.1016/j.cmet.2019.08.002

486 17. Yamashiro K, Kurita N, Urabe T, Hattori N. Role of the Gut Microbiota in Stroke
487 Pathogenesis and Potential Therapeutic Implications. *Ann Nutr Metab.* 2021;77(Suppl. 2):36-44.
488 doi:10.1159/000516398

489 18. Li Y, Ji X, Wu H, Li X, Zhang H, Tang D. Mechanisms of traditional Chinese medicine in
490 modulating gut microbiota metabolites-mediated lipid metabolism. *Journal of Ethnopharmacology*.

491 2021;278:114207. doi:10.1016/j.jep.2021.114207

492 19. Zhang R, Gao X, Bai H, Ning K. Traditional Chinese Medicine and Gut Microbiome: Their
493 Respective and Concert Effects on Healthcare. *Front Pharmacol.* 2020;11.
494 doi:10.3389/fphar.2020.00538

495 20. Fan JG, Kim SU, Wong VWS. New trends on obesity and NAFLD in Asia. *Journal of*
496 *Hepatology*. 2017;67(4):862-873. doi:10.1016/j.jhep.2017.06.003

497 21. Wang T, Guo XK, Xu H. Disentangling the Progression of Non-alcoholic Fatty Liver
498 Disease in the Human Gut Microbiota. *Front Microbiol.* 2021;12. doi:10.3389/fmicb.2021.728823

499 22. Chen J, Vitetta L. Gut Microbiota Metabolites in NAFLD Pathogenesis and Therapeutic
500 Implications. *IJMS*. 2020;21(15):5214. doi:10.3390/ijms21155214

501 23. Fang J, Yu CH, Li XJ, et al. Gut dysbiosis in nonalcoholic fatty liver disease: pathogenesis,
502 diagnosis, and therapeutic implications. *Front Cell Infect Microbiol.* 2022;12.
503 doi:10.3389/fcimb.2022.997018

504 24. Rom O, Liu Y, Liu Z, et al. Glycine-based treatment ameliorates NAFLD by modulating
505 fatty acid oxidation, glutathione synthesis, and the gut microbiome. *Sci Transl Med.* 2020;12(572).
506 doi:10.1126/scitranslmed.aaz2841

507 25. Shin J, Li T, Zhu L, et al. Obese Individuals With and Without Phlegm-Dampness
508 Constitution Show Different Gut Microbial Composition Associated With Risk of Metabolic
509 Disorders. *Front Cell Infect Microbiol.* 2022;12. doi:10.3389/fcimb.2022.859708

510 26. Li L, Li T, Liang X, et al. A decrease in Flavonifractor plautii and its product,
511 phytosphingosine, predisposes individuals with phlegm-dampness constitution to metabolic
512 disorders. *Cell Discov.* 2025;11(1). doi:10.1038/s41421-025-00789-x

513 27. Pan Y, Guo J, Hu N, et al. Distinct common signatures of gut microbiota associated with
514 damp-heat syndrome in patients with different chronic liver diseases. *Front Pharmacol.* 2022;13.
515 doi:10.3389/fphar.2022.1027628

516 28. Zhang F, Wu J, Ruan H, et al. ZeXie decoction alleviates non-alcoholic fatty liver disease

517 in rats: the study of genes, lipids, and gut microbiotas. *Biochemical and Biophysical Research*
518 *Communications*. 2022;632:129-138. doi:10.1016/j.bbrc.2022.09.097

519 29. Zhao H, Zong Y, Li W, et al. Damp-heat constitution influences gut microbiota and urine
520 metabolism of Chinese infants. *Heliyon*. 2023;9(2):e12424. doi:10.1016/j.heliyon.2022.e12424

521 30. Chen X, Tan F, Zhang H, et al. Serum cytokine profiles in phlegm-dampness constitution
522 and damp-heat constitution using proteomic antibody microarray. *European Journal of Integrative*
523 *Medicine*. 2022;52:102126. doi:10.1016/j.eujim.2022.102126

524 31. Nakagawa H, Saio T, Nagao M, et al. Conformational dynamics of a multidomain protein
525 by neutron scattering and computational analysis. *Biophysical Journal*. 2021;120(16):3341-3354.
526 doi:10.1016/j.bpj.2021.07.001

527 32. Rabe M, Toparli C, Chen YH, Kasian O, Mayrhofer KJJ, Erbe A. Alkaline manganese
528 electrochemistry studied by in situ and operando spectroscopic methods – metal dissolution, oxide
529 formation and oxygen evolution. *Phys Chem Chem Phys*. 2019;21(20):10457-10469.
530 doi:10.1039/c9cp00911f

531 33. Smalley CM, Fertel BS, McShane AJ, Cremer PC, Muir MR, Mentias A. Outcomes in
532 emergency department patients with intermediate elevations in high-sensitive cardiac troponin T.
533 *The American Journal of Emergency Medicine*. 2023;65:212-213. doi:10.1016/j.ajem.2022.12.018

534 34. Shen S, Zhong H, Zhou X, et al. Advances in Traditional Chinese Medicine research in
535 diabetic kidney disease treatment. *Pharmaceutical Biology*. 2024;62(1):222-232.
536 doi:10.1080/13880209.2024.2314705

537 35. Kumar D, Behal S, Bhattacharyya R, Banerjee D. Pseudoesterase activity of albumin: A
538 probable determinant of cholesterol biosynthesis. *Medical Hypotheses*. 2018;115:42-45.
539 doi:10.1016/j.mehy.2018.03.018

540 36. Wang S, Lin X, Zhu C, et al. Association between nonalcoholic fatty liver disease and
541 increased glucose-to-albumin ratio in adults without diabetes. *Front Endocrinol*. 2024;14.
542 doi:10.3389/fendo.2023.1287916

543 **Figure Legends**

544 **Figure 1. Gut Microbiota α -Diversity Analysis.**

545 Note: (A-D) Estimation of species diversity differences across various TCM constitution groups,
546 using the Simpson index, Chao1 index, Ace index, and Shannon index. TCM: Traditional Chinese
547 Medicine.

548 **Figure 2. Gut Microbiota α -Diversity Analysis.**

549 Note: (A-B) PCoA based on Bray-Curtis distances shows the overall microbiota composition across
550 the seven groups. The QDC group (red dots), QSC group (dark green dots), PDC group (blue dots),
551 DHC group (purple dots), BSC group (orange dots), YADC group (pink dots), and YIDC group
552 (light green dots), with each dot representing an individual sample. QDC: Qi deficiency constitution,
553 QSC: Qi stagnation constitution, PDC: Phlegm-dampness constitution, DHC: Damp-heat
554 constitution, BSC: Blood stasis constitution, YADC: Yang deficiency constitution, YIDC: Yin
555 deficiency constitution.

556 **Figure 3. Overview of Gut Microbiota in Different TCM Constitution Groups.**

557 Note: (A) Venn diagram showing the presence of ASVs across the groups. (B-E) Taxonomic
558 analysis of the microbiota communities.

559 **Figure 4. LEfSe Analysis and Correlation Between Gut Microbiota and Cytokines Across
560 Different Constitution Groups.**

561 Note: (A) Overview dendrogram of LEfSe analysis; (B) LDA scores of specifically enriched genera
562 in each group; (C) Spearman correlation analysis of microbiota-cytokine relationships. LDA: Linear
563 Discriminant Analysis.

564 **Figure 5. GC-MS Total Ion Chromatogram Analysis of Fecal Samples from
565 Phlegm-Dampness and DHC Groups.**

566 Note: (A) PDC group; (B) DHC group. GC-MS: Gas Chromatography-Mass Spectrometry, PDC:
567 Phlegm-dampness constitution, DHC: Damp-heat constitution.

568 **Figure 6. Differential Fecal Metabolites and Distribution Features Between PDC and DHC**

569 **Groups in MASLD Patients.**

570 Note: (A) PCA of fecal samples from MASLD patients in both groups. SR = DHC group; TS =
571 PDC group. (B) Volcano plot showing differential ASVs between PDC and DHC groups. (C)
572 Heatmap illustrating the relative abundance of relevant taxonomic units in the PDC and DHC
573 groups. PDC: Phlegm-dampness constitution, DHC: Damp-heat constitution, MASLD:
574 Non-alcoholic fatty liver disease.

575 **Figure 7. Bubble Chart of Metabolic Pathway Enrichment Analysis for Differential Fecal
576 Metabolites Between PDC and DHC Groups.**

577 Note: This figure presents the metabolic pathway enrichment analysis of differential metabolites
578 using MetaboAnalyst 5.0. The size of the bubbles represents the topological impact value, and the
579 color gradient from yellow to red indicates *p*-values from high to low (i.e., increasing significance).
580 The numbers represent different metabolic pathways:(1) Biosynthesis of phenylalanine, tyrosine,
581 and tryptophan;(2) Glycine, serine, and threonine metabolism;(3) Ascorbate and aldarate
582 metabolism;(4) Alanine, aspartate, and glutamate metabolism;(5) Taurine and hypotaurine
583 metabolism;(6) Arginine and proline metabolism;(7) β -Alanine metabolism;(8) Phenylalanine
584 metabolism;(9) Acetaldehyde and dicarboxylic acid metabolism;(10) Cysteine and methionine
585 metabolism;(11) Tyrosine metabolism;(12) Tricarboxylic acid cycle (TCA cycle);(13) Arginine
586 biosynthesis;(14) Pyrimidine metabolism;(15) Glutathione metabolism. The selection criteria were
587 $p < 0.05$ and an impact value > 0.1 . PDC: Phlegm-dampness constitution, DHC: Damp-heat
588 constitution.

589 **Graphic abstract. Schematic Diagram of the Differences in Gut Microbiota and Metabolic
590 Pathways Between Damp-Heat and PDC in MASLD Patients.**

591 **Figure S1. Inclusion and Exclusion Criteria for Study Participants.**

592

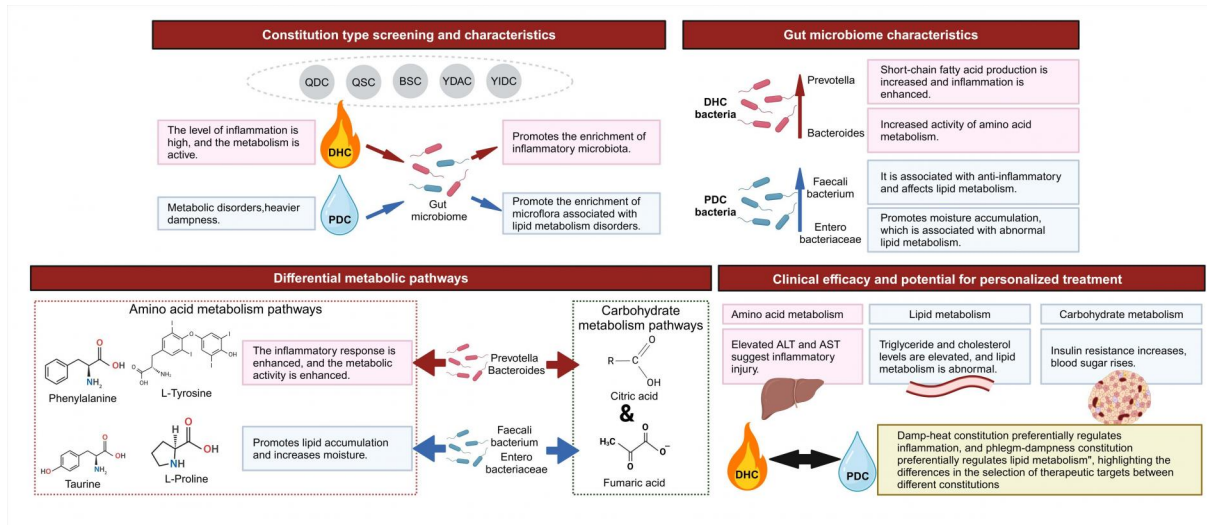


Table 1. Characteristics of the study participants.

Characteristics	Qsc(n=14)	DHC(n=28)	BSC(n=3)	YIDC(n=2)	PDC(n=2)	QDC(n=2)	YADC(n=2)	<i>p</i> -value
Sex								
Male	1	9	13	2	0	0	1	0.269
Female	2	5	15	1	1	2	0	
Age	48.57±14.92	50.11±12.33	65.67±8.02	53±1.21	65±5.66	61±2.13	65±2.83	0.164
weight(kg)	75.04±16.28	71.96±11.23	76.03±17.53	73.37±0.04	57.95±6.43	83.47±16.22	64±5.66	0.484
BMI (kg/m ²)	26.23±4.01	25.59±3.51	27.52±3.72	33.97±0	22.9±2.14	28.51±5.09	26.63±4.52	0.073
TC	4.89±1.32	4.89±1.31	4.55±0.96	4.32±0.04	3.55±0.84	4.75±0.09	5.18±0.25	0.822
TG	2.29±1.29	2.56±1.41	1.91±0.26	5.62±0.04	3.8±1.67	1.1±0.48	1.44±0.13	0.014
HDL-C	1.11±0.22	1.01±0.27	1.04±0.1	0.61±0.04	0.56±0.04	1.05±0.18	1.24±0.21	0.02
LDL-C	2.74±1.21	3.21±1.31	2.29±0.36	2.57±0.04	2.22±0.78	3.07±0.07	3.33±0.35	0.695
GLU	6.37±2.15	7.96±3.46	5.96±1.55	4.56±0.04	9.78±2.07	4.72±0.76	8.4±1.75	0.234
ALT	26.25±22.19	28.73±21.09	33.67±31.56	14.97±0.04	26.5±14.85	57.4260.06	19±2.83	0.609
AST	19.36±6.29	20.08±7.71	26±22.52	15.97±0.04	26±7.07	25.97±18.34	19±0.23	0.721

Table 2. Fecal metabolomic analysis of differential metabolites in DHC and PDC groups.

NO.	Metabolites	FondChang	PValue
1	lyxose	0.48965	0.010618
2	arabitol	0.31528	0.033477
3	iminodaceticacid	0.57179	0.034533
4	gentisicacid	0.51515	0.058056
5	quinicacid	0.094409	0.06064
6	putrescine	1.8711	0.060696
7	sucrose	0.44471	0.067313
8	1-2-4-benzenetriol	0.67369	0.067334
9	succinicacid	0.27505	0.072758
10	4-hydroxy-3-methoxybenzoicacid	0.37971	0.07803
11	4-nitrocatechol	1.8635	0.08902
12	glycerol-1-phosphate	0.71656	0.10617
13	xanthosine	0.49592	0.11173
14	O-phosphoserine	1.5873	0.13149
15	uracil	0.89585	0.13815
16	4-pyridoxicacid	0.20601	0.14978
17	pyrogallol	0.15497	0.15134
18	caffeicacid	0.53365	0.20037
19	gallicacid	0.21349	0.20443

20	4-hydroxybenzoicadd	0.83878	0.21276
21	3-(3-hydroxyphenyl)propionicacid	0.82316	0.21422
22	mannitol	0.67599	0.22035
23	3-hydroxypropionicadd	0.61144	0.22793
24	3-phenyllacticacid	1.0008	0.25102
25	sedoheptulose	22.023	0.25135
26	1-hexadecanol	0.29505	0.26001
27	threonine	1.1805	0.26133
28	myo-inositol	0.48606	0.26161
29	taurine	1.5051	0.26594
30	catechin	0.11953	0.28396
31	trans-3-hydroxy-L-proline	2.5432	0.28397
32	3-4-dihydroxybenzoicacd	0.16982	0.30015
33	tyramine	0.82997	0.32175
34	daidzein	0.10697	0.34115
35	N-acetyl-D-galactosamine	0.85874	0.34495
36	N-methylalanine	0.48751	0.35057

Table 3. Results of pathway enrichment analysis of differential metabolites in serum samples.

No.	pathway	P	Impact	Metabolites
1	Phenylalanine,tyrosine and tryptophan biosynthesis	0.0095387	1	L-Phenylalanine;L-Tyrosine
2	Glycine,serine and threonine metabolism	0.00026861	0.64073	L-Serine;Glycine,O-Phosphorylated
3	Ascorbate and aldarate metabolism	0.0047181	0.52381	Inositol;D-Glucuronide:D-Gluconate
4	Alanine,aspartate and glutamate metabolism	0.00072173	0.50962	L-Aspartic acid;;L-Glutamic acid;4-Aminobutyrate;Citrate,Fumarate,Succinate
5	Taurine and hypotaurine metabolism	0.039993	0.42857	L-Cysteine;Taurine
6	Arginine and proline metabolism	0.0028753	0.41627	4-Aminobutyrate;putrescine;trans-3-Hydroxy-L-proline;L-Proline,
7	beta-Alanine metabolism	0.0093132	0.39925	L-Glutamic acid:L-Omithine 3-Hydroxypropionate;β-Alanine L-Aspartic Acid;uracil
8	Phenylalanine metabolism	0.039993	0.35714	L-Phenylalanine;L-Tyrosine
9	Glyoxylate and dicarboxylate metabolism	0.0015238	0.25927	Citrate;(S)-Malic Acid;L-Serine;Glydine;L-Glutamic Acid;D-Glycerate
10	Cysteine and methionine metabolism	0.043963	0.22222	L-serine;L-methionine,L-cysteine; O-phosphorylated L-serine
11	Tyrosine metabolism	0.026728	0.20072	L-adranaline;L-tyrosine:tyramine;fumarate;2,5-dihydroxybenzoate
12	Citate cycle (TCA cycle)	0.0077773	0.19704	Succinate (S)-Malate Citate,Fumarate

13	Arginine biosynthesis	0.00015406	0.17766	L-Glutamic Acid;L-Aspartic Acid;L-Omithine;Urea;Fumarate
14	Pyrimidine metabolism	0.019897	0.17576	Uridine;Thymine;Orotate;Uracil;β-Alanine
15	Glutathione metabolism	0.00072173	0.1261	Glycine;L-Cysteine;L-Glutamic acid;Methylphenidate L-Omithine:Putescine

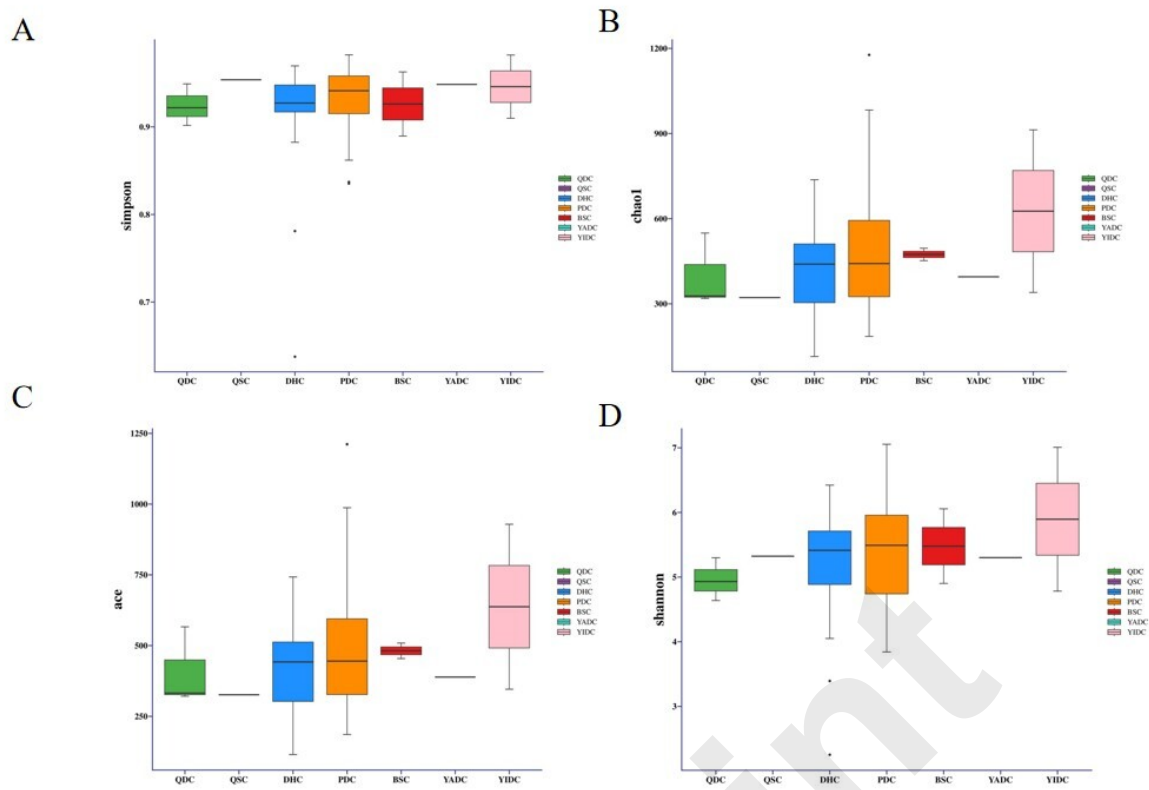


Figure 1. Gut Microbiota α -Diversity Analysis.

Note: (A-D) Estimation of species diversity differences across various TCM constitution groups, using the Simpson index, Chao1 index, Ace index, and Shannon index. TCM: Traditional Chinese Medicine.

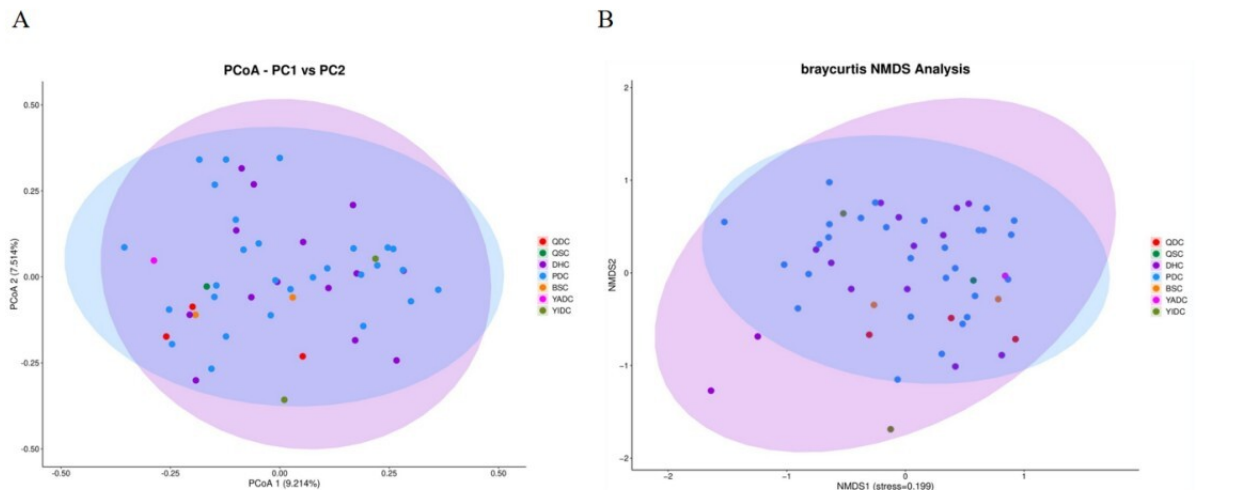


Figure 2. Gut Microbiota α -Diversity Analysis.

Note: (A-B) PCoA based on Bray-Curtis distances shows the overall microbiota composition across the seven groups. The QDC group (red dots), QSC group (dark green dots), PDC group (blue dots), DHC group (purple dots), BSC group (orange dots), YADC group (pink dots), and YIDC group (light green dots), with each dot representing an individual sample. QDC: Qi deficiency constitution, QSC: Qi stagnation constitution, PDC: Phlegm-dampness constitution, DHC: Damp-heat constitution, BSC: Blood stasis constitution, YADC: Yang deficiency constitution, YIDC: Yin deficiency constitution.

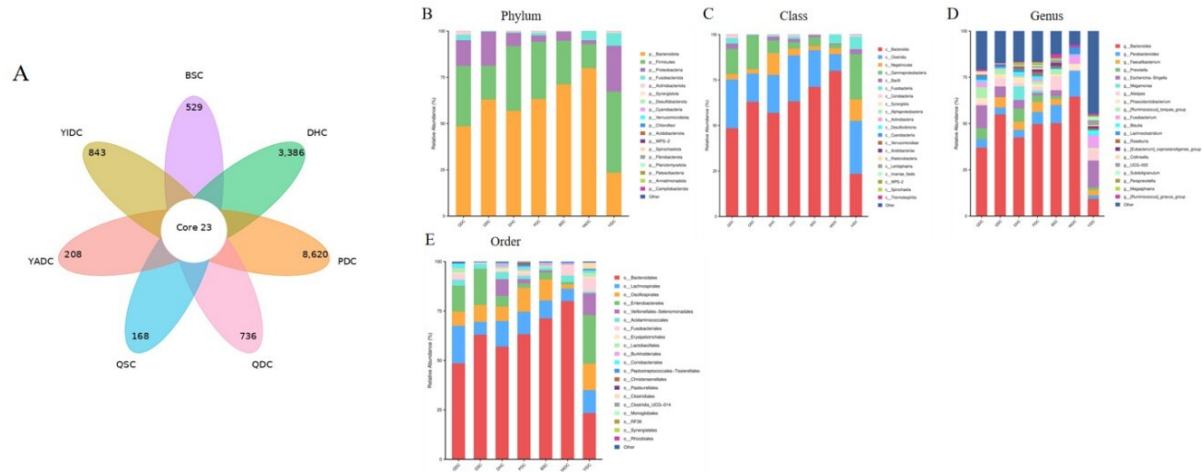


Figure 3. Overview of Gut Microbiota in Different TCM Constitution Groups.

Note: (A) Venn diagram showing the presence of ASVs across the groups. (B-E) Taxonomic analysis of the microbiota communities.

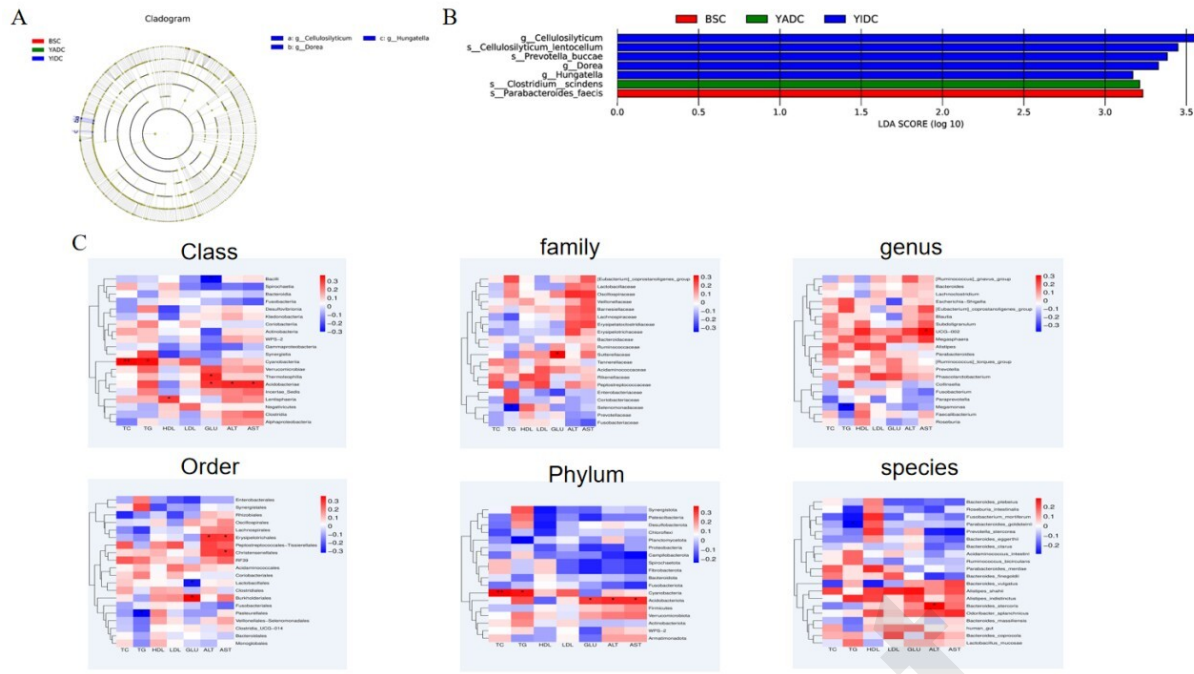
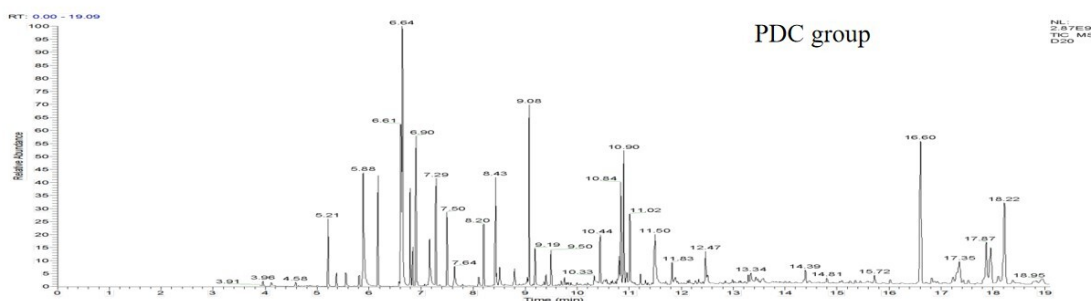


Figure 4. LEfSe Analysis and Correlation Between Gut Microbiota and Cytokines Across Different Constitution Groups.

Note: (A) Overview dendrogram of LEfSe analysis; (B) LDA scores of specifically enriched genera in each group; (C) Spearman correlation analysis of microbiota-cytokine relationships. LDA: Linear Discriminant Analysis.

A



B

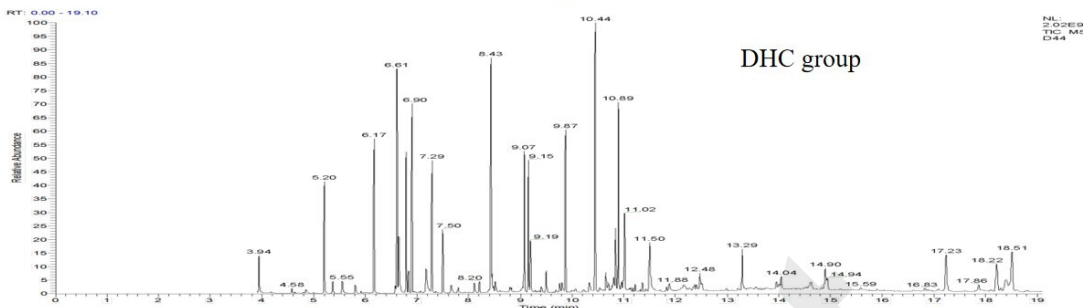


Figure 5. GC-MS Total Ion Chromatogram Analysis of Fecal Samples from Phlegm-Dampness and DHC Groups.

Note: (A) PDC group; (B) DHC group. GC-MS: Gas Chromatography-Mass Spectrometry, PDC: Phlegm-dampness constitution, DHC: Damp-heat constitution.

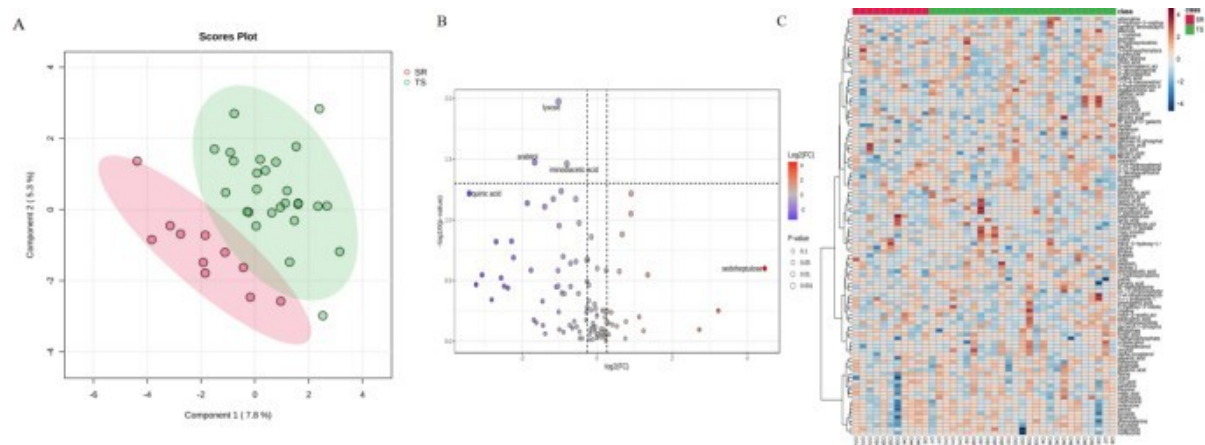


Figure 6. Differential Fecal Metabolites and Distribution Features Between PDC and DHC Groups in MASLD Patients.

Note: (A) PCA of fecal samples from MASLD patients in both groups. SR = DHC group; TS = PDC group. (B) Volcano plot showing differential ASVs between PDC and DHC groups. (C) Heatmap illustrating the relative abundance of relevant taxonomic units in the PDC and DHC groups. PDC: Phlegm-dampness constitution, DHC: Damp-heat constitution, MASLD: Non-alcoholic fatty liver disease.

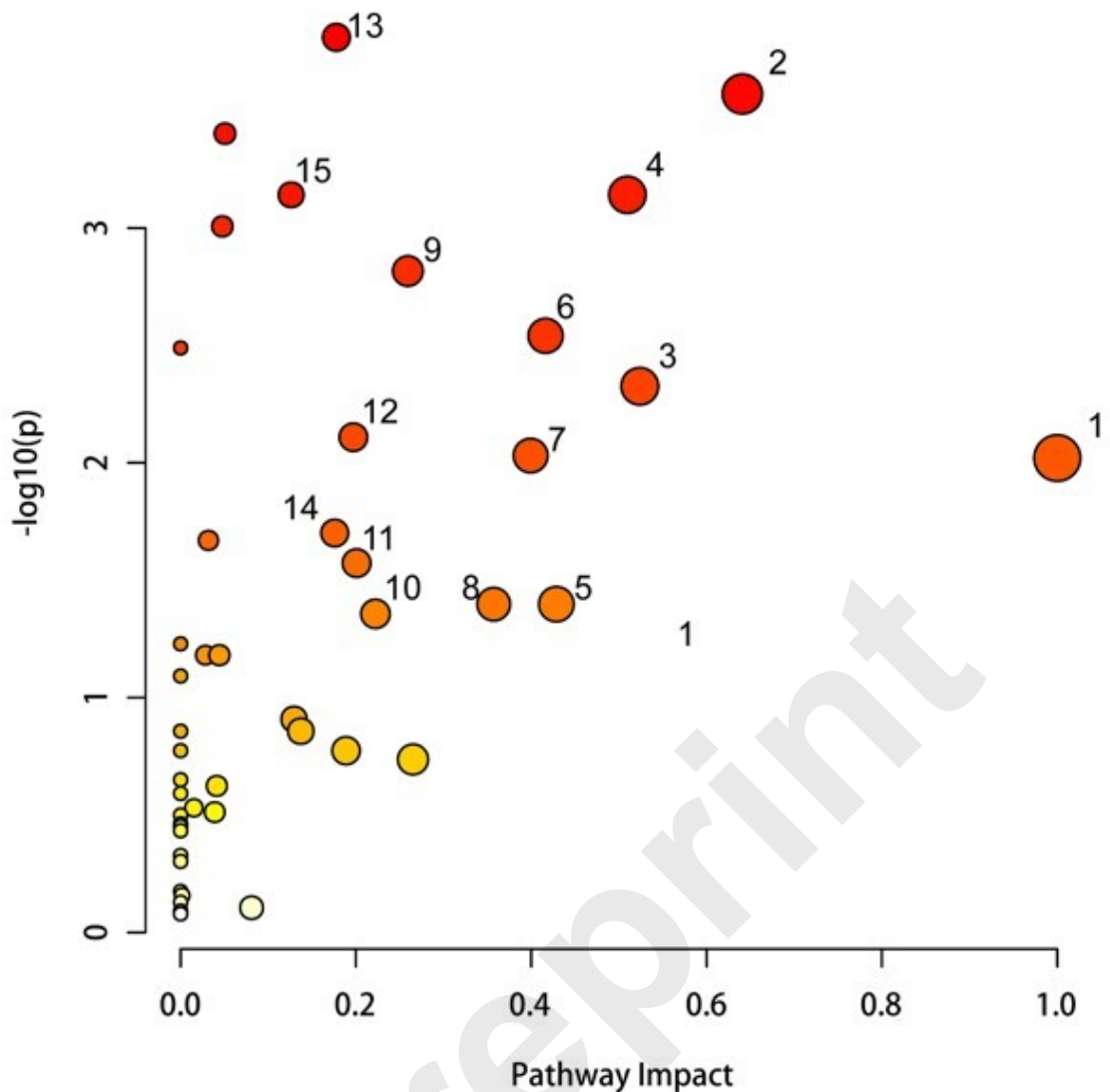


Figure 7. Bubble Chart of Metabolic Pathway Enrichment Analysis for Differential Fecal Metabolites Between PDC and DHC Groups.

Note: This figure presents the metabolic pathway enrichment analysis of differential metabolites using MetaboAnalyst 5.0. The size of the bubbles represents the topological impact value, and the color gradient from yellow to red indicates p-values from high to low (i.e., increasing significance). The numbers represent different metabolic pathways: (1) Biosynthesis of phenylalanine, tyrosine, and tryptophan; (2) Glycine, serine, and threonine metabolism; (3) Ascorbate and aldarate metabolism; (4) Alanine, aspartate, and glutamate metabolism; (5) Taurine and hypotaurine metabolism; (6) Arginine and proline metabolism; (7) β -Alanine metabolism; (8) Phenylalanine metabolism; (9) Acetaldehyde and dicarboxylic acid metabolism; (10) Cysteine and methionine metabolism; (11) Tyrosine metabolism; (12) Tricarboxylic acid cycle (TCA cycle); (13) Arginine biosynthesis; (14) Pyrimidine metabolism; (15) Glutathione metabolism. The selection criteria were $p < 0.05$ and an impact value > 0.1 . PDC: Phlegm-dampness constitution, DHC: Damp-heat constitution.

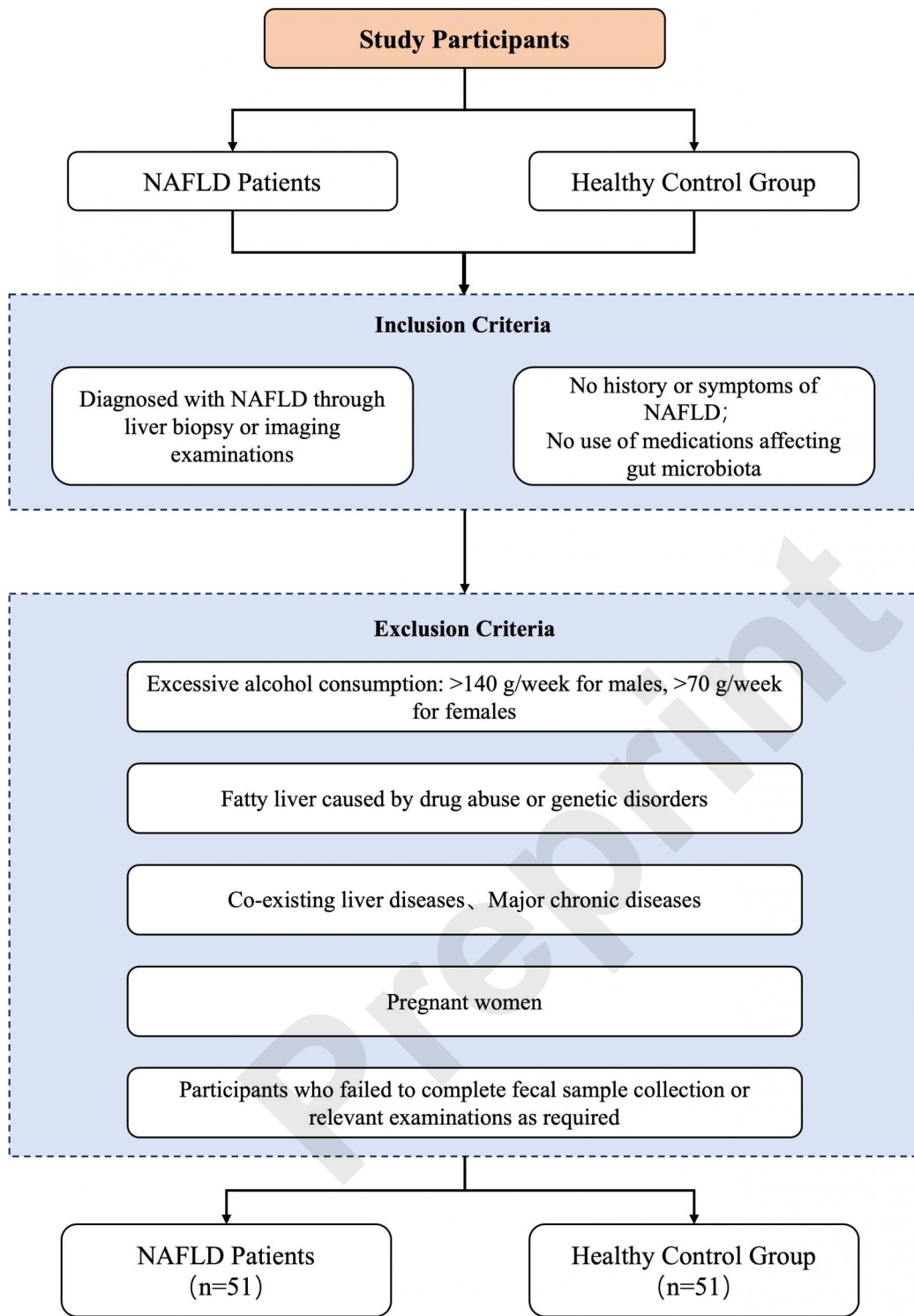


Figure S1. Inclusion and Exclusion Criteria for Study Participants.